

## Probing Phonon Dispersion Relations of Graphite by Double Resonance Raman Scattering

R. Saito,<sup>1</sup> A. Jorio,<sup>2</sup> A. G. Souza Filho,<sup>2,5</sup> G. Dresselhaus,<sup>3</sup> M. S. Dresselhaus,<sup>2,4</sup> and M. A. Pimenta<sup>6</sup>

<sup>1</sup>Department of Electronic Engineering, University of Electro-Communications, Chofu, Tokyo 182-8585 Japan

<sup>2</sup>Department of Physics, Massachusetts Institute of Technology, Cambridge, Massachusetts 02139-4307

<sup>3</sup>Francis Bitter Magnet Laboratory, Massachusetts Institute of Technology, Cambridge, Massachusetts 02139-4307

<sup>4</sup>Department of Electrical Engineering and Computer Science, Massachusetts Institute of Technology, Cambridge, Massachusetts 02139-4307

<sup>5</sup>Departamento de Física, Universidade Federal do Ceará, Fortaleza-CE 60455-760, Brazil

<sup>6</sup>Departamento de Física, Universidade Federal de Minas Gerais, Belo Horizonte-MG 30123-970, Brazil

(Received 13 August 2001; published 20 December 2001)

The phonon dispersion relations of graphite can be probed over a wide range of the Brillouin zone by double resonance Raman spectroscopy. The double resonance Raman process provides us with new assignments for the dispersive and nondispersive features observed in the Raman spectra of disordered graphite and carbon nanotubes, some features having been incorrectly assigned previously, or not assigned at all.

DOI: 10.1103/PhysRevLett.88.027401

PACS numbers: 78.30.Na, 78.66.Tr

The phonon dispersion relations provide us with basic information about the physical properties of crystalline solids. Generally, inelastic neutron scattering is considered to be the experimental tool of choice for measuring the phonon dispersion relations over large regions of the Brillouin zone (BZ) and over most of the phonon frequency range. Here we show that inelastic light scattering by phonons, that is, Raman spectroscopy, can also provide a powerful tool for determining the phonon dispersion relations, particularly in low dimensional materials, when combined with information about the electronic structure.

In the Raman spectra of disordered graphite [1] and single wall carbon nanotubes (SWNTs) [2], in addition to the Raman-allowed graphite peak, low intensity reproducible features in the Raman spectra are frequently observed. A well-known dispersive spectral feature is the disorder-induced *D* band which appears at around  $1350\text{ cm}^{-1}$  for laser excitation at about 2.41 eV. The *D* band frequency is highly dispersive and increases with increasing laser energy  $E_{\text{laser}}$  by  $44\text{--}51\text{ cm}^{-1}/\text{eV}$  for various graphite and  $sp^2$  carbon materials [3–5] and by  $53\text{ cm}^{-1}/\text{eV}$  for SWNTs [6], respectively. This dispersive behavior is known to be due to a  $k$ -selective resonance process, as suggested by various groups [3,4,7]. Recently, Thomsen and Reich proposed a model for the origin of the *D* band in terms of a double resonance process [8]. The double resonance effect occurs when both the scattered intermediate state and the initial (or final) state are actual electronic states. Thomsen and Reich applied the double resonance processes to one of the six phonon branches of the dispersion relations of graphite, the branch which is responsible for the *D* band. This model can, however, be extended to other phonon branches to predict other dispersive phonon modes in graphite, or to identify other dispersive phonon modes that have been previously observed in resonance Raman experiments in  $sp^2$  carbons [4,6,9–14]. In this Letter, we have succeeded in assigning

almost all previously unassigned phonon modes in  $sp^2$  carbons. This idea can also be generally applied to other solids to identify phonon dispersion relations that can be observed by resonance Raman spectroscopy.

In the Stokes (phonon emission) process, an electron with momentum  $k$  [and electron energy  $E^i(k)$ ] is excited by the incident laser photon in an electron-hole creation process. The electron is then scattered by emitting a phonon with momentum  $q$  to the state with momentum  $k + q$  [and energy  $E(k + q)$ ], then scattered again, back to  $k$  [ $E^f(k)$ ] to recombine with a hole. In the one-phonon emission (first-order Raman) Stokes process, one of the two scattering processes ( $k \rightarrow k + q, k + q \rightarrow k$ ) is *inelastic* with a phonon emission process, and the other is an *elastic* scattering process mediated by the defect. Furthermore, there are two possibilities for the resonance conditions, either  $E^i(k)$  or  $E^f(k)$  is resonant with an electronic state. Thus we can expect four different double resonance Raman processes, as shown in Fig. 1, which can each make important contributions to the Raman intensity. When we measure the energy from that of the valence band at  $k$ , the four resonant conditions of Fig. 1 can be expressed, respectively, by

$$\begin{aligned} \mathbf{E}^i(\mathbf{k}) &= E_{\text{laser}}, & \mathbf{E}(\mathbf{k} + \mathbf{q}) &= \mathbf{E}^i(\mathbf{k}) - \hbar\omega_{\text{ph}}(q), \\ E^f(k) &= \mathbf{E}(\mathbf{k} + \mathbf{q}), \end{aligned} \quad (1)$$

$$\begin{aligned} E^i(k) &= E_{\text{laser}}, & \mathbf{E}(\mathbf{k} + \mathbf{q}) &= E^i(k) - \hbar\omega_{\text{ph}}(q), \\ \mathbf{E}^f(\mathbf{k}) &= \mathbf{E}(\mathbf{k} + \mathbf{q}), \end{aligned} \quad (2)$$

$$\begin{aligned} \mathbf{E}^i(\mathbf{k}) &= E_{\text{laser}}, & \mathbf{E}(\mathbf{k} + \mathbf{q}) &= \mathbf{E}^i(\mathbf{k}), \\ E^f(k) &= \mathbf{E}(\mathbf{k} + \mathbf{q}) - \hbar\omega_{\text{ph}}(-q), & \text{and} \end{aligned} \quad (3)$$

$$\begin{aligned} E^i(k) &= E_{\text{laser}}, & \mathbf{E}(\mathbf{k} + \mathbf{q}) &= E^i(k), \\ \mathbf{E}^f(\mathbf{k}) &= \mathbf{E}(\mathbf{k} + \mathbf{q}) - \hbar\omega_{\text{ph}}(-q). \end{aligned} \quad (4)$$

Here the boldface means that there exists a *real*

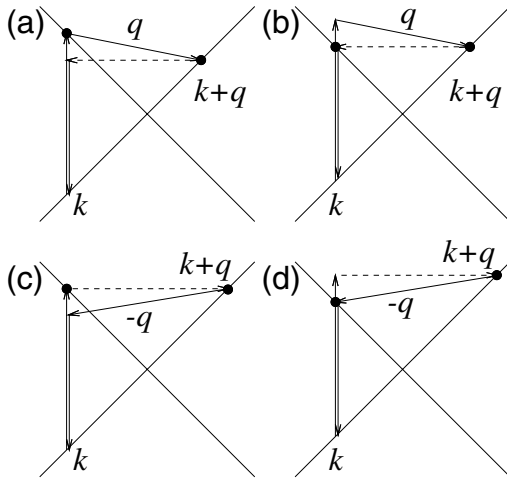


FIG. 1. Four different second-order double resonance Stokes processes. For each process, the dashed lines denote an elastic scattering process and black dots are shown for the resonant points. For the two-phonon second-order processes, the dashed line of each figure is changed to be an inelastic phonon emission process and thus only the (a) and (d) processes are possible for two-phonon scattering processes.

electronic state which satisfies the resonance condition. For all cases,  $E(k + q)$  is always one of the resonant electronic states, and either  $E^i(k)$  or  $E^f(k)$  is the second resonant state (yielding the double resonance condition). In the anti-Stokes process (phonon absorption), we consider the time-reversal counterpart of the corresponding Stokes process, and thus we have four corresponding anti-Stokes processes. Equations (1) to (4) are thus different for Stokes and anti-Stokes processes, giving rise to different frequencies compared to the corresponding Stokes and anti-Stokes processes, as observed experimentally for the dispersive modes in  $sp^2$  materials [9,10]. For a two-phonon Stokes process, such as the  $G'$  band ( $\omega_{G'} \sim 2\omega_D$ ), the elastic scattering process denoted by a dashed line in Fig. 1 is changed to an inelastic phonon emission process. Then, only cases (1) and (4) are possible for two-phonon double resonance processes.

For  $E_{\text{laser}} < 3.0$  eV, the energy contours of  $E = E^i(k)$ ,  $E(k + q)$ , and  $E^f(k)$  are circles around the hexagonal  $K$  or  $K'$  corner points in the first BZ of two-dimensional (2D) graphite, as shown by solid circles in Fig. 2. Three circles centered on the  $K$  (or  $K'$ ) points are identical circles in the periodic  $k$  space. When we consider a  $k$  point on the circle  $E = E(k)$  around the upper-right  $K$  point, energy and momentum conservation selects two possible cases for the scattered  $k + q$  electronic states on two  $E = E(k + q)$  circles: (i)  $k + q$  is around the same  $K$  point in the BZ, and (ii)  $k + q$  is around the inequivalent  $K'$  point, as shown in Fig. 2. Hereafter, we refer to the two cases, respectively, as intravalley ( $K \leftrightarrow K$ , or  $K' \leftrightarrow K'$ ) and intervalley ( $K \leftrightarrow K'$ ) scattering.

Intervalley scattering requires a phonon  $q$  vector which connects  $E(k)$  around the  $K$  point to  $E(k + q)$  around the

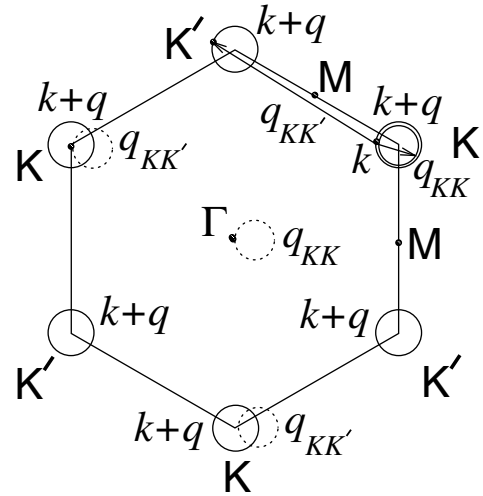


FIG. 2. Energy contours of  $E = E^i(k)$ ,  $E(k + q)$ , and  $E^f(k)$  are shown as solid circles around the hexagonal corners of the  $K$  or  $K'$  points in the Brillouin zone of two-dimensional graphite. Dotted circles around the  $K$  and  $\Gamma$  points give all possible  $q$  vectors for a given  $k$  vector shown near the upper-right  $K$  point.

$K'$  point. When we measure all such  $q_{KK'}$  vectors from the  $\Gamma$  point, the ends of these  $q_{KK'}$  vectors for a given  $k$  fall on the dotted circle near the  $K$  points, as shown in Fig. 2. The phonon modes with  $q_{KK'}$  vectors around the  $K$  point are relevant to the  $D$ -band Raman spectra. The intravalley scattering has phonon  $q_{KK}$  vectors near the  $\Gamma$  point and thus this scattering is related to the  $\Gamma$  point phonon frequency. When we calculate the resonant  $q$  vectors for a given  $k$  vector, the dotted circles in the first BZ almost touch the  $K$  point, or the  $\Gamma$  point in Fig. 2. In the case of elastic scattering [ $E(k) = E(k + q)$ ], the dotted circles touch the  $K$  or the  $\Gamma$  points, and, in the case of phonon emission scattering [ $E(k + q) = E(k) - \hbar\omega_{\text{ph}}$ ], the circles do not touch and are slightly displaced from these points by the phonon energy  $\hbar\omega_{\text{ph}}$ .

Since the phonon dispersion is isotropic around the  $K$  or the  $\Gamma$  points, except for the trigonal warping effect [15], the corresponding phonon frequency depends only on the distance of the  $q$  vectors from the  $K$  or  $\Gamma$  points. Thus, the distance of the  $q$  vectors, measured from the  $K$  (or  $\Gamma$ ) point,  $|q - K|$  ( $|q|$ ), can vary from 0 to  $2|k - K|$ , where  $K$  is the wave vector of the  $K$  point. When we consider the distribution of possible  $q$  distances, a 1D Van Hove singularity occurs at  $|q - K| = 2|k - K|$  or  $|q| = 2|k - K|$  in the density of possible  $q$  distances. Thus, the  $D$ -band frequency will be selected for  $q$  vectors which satisfy  $|q - K| = 2|k - K|$ . The factor 2 in  $|q - K| = 2|k - K|$  might be modified somewhat by the trigonal warping effect [15]. When  $k$  is placed on the energy contour, the dotted circle rotates around the  $K$  (or  $\Gamma$ ) point, while keeping contact with the  $K$  ( $\Gamma$ ) point. The calculated result shows some singularlike behavior also at  $|q - K| = 0$  (or at  $|q| = 0$ ), which results from the many possible  $q$  values around the  $K$  (or  $\Gamma$ ) point which give the

same frequency because of the flat phonon energy dispersion curves, although the 2D phonon density of states is not singular at the  $K$  (or  $\Gamma$ ) point. Since there exist weak features of Raman intensity for some phonon modes for  $|q - K| = 0$  (or at  $|q| = 0$ ) [1], we need to discuss the scattering matrix element for evaluating these peaks, and this will be a future problem.

The Raman frequency of the double resonance effect is generally observed as an intersection of the six phonon energy dispersion curves of 2D graphite with  $|q - K| = 2|k - K|$  (or  $|q| = 2|k - K|$ ) or with  $|q - K| = 0$  (or  $|q| = 0$ ). It is easy to distinguish the peaks at  $|q| = 0$  from those at  $|q| = 2|k - K|$ , since the former do not change their frequency by varying the laser excitation energy. Since  $|q| = 2|k - K|$  is not a zone-center or zone-edge phonon mode, we can change both the  $k$  and  $q$  values by changing  $E_{\text{laser}}$ . Thus by using electronic structure information, we can determine phonon dispersion relations around the  $K$  or the  $\Gamma$  points. Such spectra should have much lower intensity than the first-order zone-center Raman modes. Nevertheless, some small intensity peaks that have been known for many years to be present in the Raman spectra of  $sp^2$  carbons can now be assigned very well by the double resonance process described above.

In Fig. 3, we plot vs  $\omega_{\text{ph}}$  the calculated density of  $(k, q)$  pairs which satisfy one of the four double resonance conditions of Fig. 1, for the five laser energies 3(a) 0.93 to 3(e) 2.41 eV which are often used in resonance Raman experiments. When  $E_{\text{laser}}$  increases, the number of allowed  $k$  vectors [the length of the contour  $E = E(k)$ ]

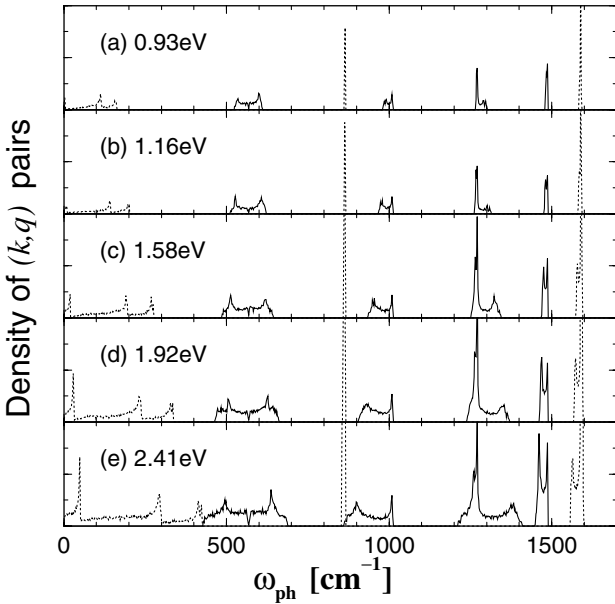


FIG. 3. Calculated dependence of  $\omega_{\text{ph}}$  of the density of  $(k, q)$  pairs which satisfy one of the four double resonance conditions. Solid and dotted lines correspond to phonon modes around the  $K$  and  $\Gamma$  points, respectively. The assignment of the 2D graphite phonon modes is given in Fig. 4 and in the text.

increases. Here we use the phonon dispersion relation calculation [16,17] and a simple tight-binding electronic energy calculation with tight-binding overlap energy parameter  $\gamma_0 = 3.033$  eV and  $s = 0.129$  [17] for asymmetric valence and conduction bands. We also calculated the  $(k, q)$  pairs with  $\gamma_0 = 2.89$  eV and  $s = 0.0$  which is known to reproduce very well the Raman spectra of isolated SWNTs [18] on an insulating substrate [15], but no substantial difference was found in the results for the peak frequency between the two parameter sets for  $E_{\text{laser}} < 3.0$  eV. Solid and dotted lines in Fig. 3 correspond to the resonance condition from the  $K$  and  $\Gamma$  points, respectively. The Raman intensity is proportional to the square of the density of  $(k, q)$  pairs in Fig. 3, if we neglect for simplicity any dependence of the matrix element of the inelastic and elastic scattering processes on  $k$  and  $q$ .

Figure 4(a) plots the  $E_{\text{laser}}$  dependence of the frequency of the peaks in the density of  $(k, q)$  pairs (see Fig. 3). The upper horizontal axis of the figure correlates the  $E_{\text{laser}}$  (the lower horizontal axis) values with the phonon wave vector  $q$  related to each peak. It is noted that the linear relationship between  $E_{\text{laser}}$  and  $q$  is valid for  $E_{\text{laser}} \leq 3.0$  eV. Solid and open circles correspond to the phonon modes around the  $K$  ( $q_{KK'}$ ) and the  $\Gamma$  ( $q_{KK}$ ) points, respectively. Along the  $\Gamma$ - $K$  direction,  $q_{KK}$  changes from  $\Gamma$  to  $\sim K/4$  by increasing  $E_{\text{laser}}$  from 0 to 3.0 eV, while  $q_{KK'}$  changes from

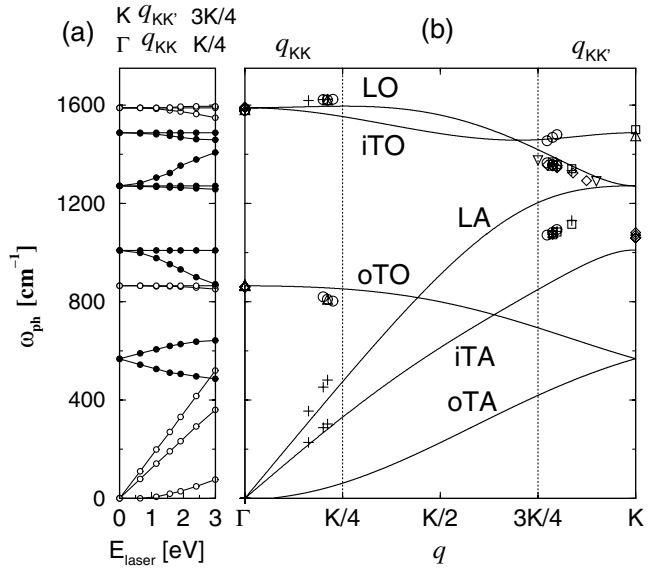


FIG. 4. (a) Calculated Raman frequencies for the double resonance condition in 2D graphite as a function of  $E_{\text{laser}}$  (bottom horizontal axis) and  $q$  vector along  $\Gamma$ - $K$  (top horizontal axis). Solid and open circles correspond to phonon modes around the  $K$  and the  $\Gamma$  points, respectively. (b) The six graphite phonon dispersion curves (lines) [16,17] and experimental Raman observations (symbols) placed according to the double resonance theory. “○”—(PG) Ref. [11]; “□”—(C-HOPG) Ref. [10], “△”—(HOPG) Refs. [11,12]; “◇”—(SWNT) Refs. [6,13,14]; “+”—(GW) Ref. [9]; “▽”—(MG) Ref. [4]. See text for notation for  $sp^2$  carbons.

$K$  to  $\sim 3K/4$ , so that  $1/2$  of the BZ along  $\Gamma-K$  is probed by this range of  $E_{\text{laser}}$ . Figure 4(b) shows the graphite phonon dispersion relations in the  $\Gamma-K$  direction [16,17]. Vertical dotted lines show limits for the  $q_{KK}$  and  $q_{KK'}$  wave vectors imposed by  $E_{\text{laser}} \leq 3.0$  eV. By comparing Figs. 4(a) and 4(b), it is easy to correlate the peaks in the density of  $(k, q)$  pairs with the six different phonon branches in graphite, as discussed above.

By using the  $E_{\text{laser}} \leftrightarrow q$  relations given in Fig. 4(a), we can take experimental values from several published papers giving Raman frequencies observed using different laser lines for various  $sp^2$  carbons and plot all these data points in Fig. 4(b), as is usually done for inelastic neutron scattering determinations of the phonon branches. The symbols in Fig. 4(b) show experimental values for highly ordered pyrolytic graphite (HOPG) [11,12], pyrolytic graphite (PG) [11], single wall carbon nanotubes [6,13,14],  $^{12}\text{C}$  ion implanted HOPG (C-HOPG) [10], microcrystalline graphite (MG) [4], and graphite whiskers (GW) [9].

This approach allows us to assign several Raman features previously observed for these materials. For example, recently Tan *et al.* reported two dispersive relatively lower phonon frequency modes in GW [9], which we assign to two of the three acoustic modes [iTA and LA, in Fig. 4(b)], which are resonant by an intravalley scattering process. The frequency of the lowest acoustic branch at  $49 \text{ cm}^{-1}$  (oTA) for  $E_{\text{laser}} = 2.41$  eV should be difficult to observe in a Raman experiment. Here the symbols “i” and “o” denote in-plane and out-of-plane phonon modes, respectively. The features around 1480 and  $864 \text{ cm}^{-1}$  are assigned for the first time to the iTO and oTO phonon branches, respectively. Furthermore, the broad weak signal around  $1580 \text{ cm}^{-1}$ , which is a background of the strong  $G$ -band peaks, is assigned to the LO phonon branch near the  $\Gamma$  point. The calculated frequencies and their dispersion are in excellent agreement with the experimental results for all of these features [see Fig. 4(b)].

However, the phonon modes between 1000 and  $1200 \text{ cm}^{-1}$  along  $\Gamma-K$  do not fit well to the calculated phonon dispersion data. We tentatively assign points  $1070 \text{ cm}^{-1}$  around  $3K/4$  and  $K$  in Fig. 4(b) to the LA and iTA phonon branches, respectively. The force constants that are used in the phonon dispersion calculation of Fig. 4(b) (solid lines) are fitted to neutron inelastic scattering data [19]. However, it is known that the region  $1000 < \omega < 1200 \text{ cm}^{-1}$  around the  $K$  points has not been measured by neutron scattering due to experimental limitations of the technique. Therefore, the double resonance Raman scattering measurements may provide an alternative experimental result that cannot be accurately probed by other experimental techniques.

All newly assigned phonon modes not only satisfy the observed phonon frequencies but also satisfy the sign and magnitude of  $\partial\omega_{\text{ph}}/\partial E_{\text{laser}}$ , thus confirming that these

small intensity Raman peaks come from the same basic double resonance, first-order phonon inelastic scattering process. For  $E_{\text{laser}} \leq 3.0$  eV, we can determine the phonon dispersion relation from the  $\Gamma$  and the  $K$  points covering a large area of the 2D graphite BZ. Since the assumption that the phonon energy dispersion is almost symmetric around the  $K$  and the  $\Gamma$  points will no longer be valid as  $E_{\text{laser}}$  increases beyond  $\sim 3.0$  eV, we have limited our discussion to this lower  $E_{\text{laser}}$  range. To get further information about the phonon dispersion relations by Raman spectroscopy, we need to consider a special experimental geometry, commonly used in photoelectron spectroscopy, for selecting the scattered  $k + q$  electron momentum or the corresponding  $q$  momentum of the phonon. Such a study will be a challenging subject for future Raman spectroscopy experiments.

The authors deeply thank Professor Ping-Heng Tan for providing his unpublished data on the lower frequency dispersive phonon modes. R. S. acknowledges a Grant-in-Aid (No. 13440091) from the Ministry of Education, Japan. A. J. and A. G. S. F. acknowledge support from the Brazilian agencies CNPq and CAPES. The MIT authors acknowledge support under NSF Grants No. DMR 01-16042, No. INT 98-15744, and No. INT 00-00408. M. A. P. acknowledges CNPq No. 910120/99-4.

- 
- [1] P. Lespade, R. Al-Jishi, and M. S. Dresselhaus, Carbon **20**, 427 (1982).
  - [2] A. M. Rao *et al.*, Science **275**, 187 (1997).
  - [3] M. J. Matthews *et al.*, Phys. Rev. B **59**, R6585 (1999).
  - [4] I. Pócsik *et al.*, J. Non-Cryst. Solids **227–230**, 1083 (1998).
  - [5] Y. Wang, D. C. Aolsmeyer, and R. L. McCreery, Chem. Mater. **2**, 557 (1990).
  - [6] M. A. Pimenta *et al.*, Braz. J. Phys. **30**, 423 (2000).
  - [7] A. C. Ferrari and J. Robertson, Phys. Rev. B **61**, 14095 (2000); **64**, 075414 (2001).
  - [8] C. Thomsen and S. Reich, Phys. Rev. Lett. **85**, 5214 (2000).
  - [9] P. H. Tan *et al.*, Phys. Rev. B **64**, 214301 (2001).
  - [10] P. H. Tan *et al.*, Phys. Rev. B **58**, 5435 (1998).
  - [11] Y. Kawashima *et al.*, Phys. Rev. B **52**, 10053 (1995).
  - [12] Y. Kawashima *et al.*, Phys. Rev. B **59**, 62 (1999).
  - [13] L. Alvarez *et al.*, Chem. Phys. Lett. **320**, 441 (2000).
  - [14] P. H. Tang *et al.*, Appl. Phys. Lett. **75**, 1524 (1999).
  - [15] R. Saito, G. Dresselhaus, and M. S. Dresselhaus, Phys. Rev. B **61**, 2981 (2000).
  - [16] R. Saito *et al.*, Phys. Rev. B **57**, 4145 (1998).
  - [17] R. Saito, G. Dresselhaus, and M. S. Dresselhaus, *Physical Properties of Carbon Nanotubes* (Imperial College Press, London, 1998).
  - [18] A. G. Souza Filho *et al.*, Phys. Rev. B **63**, 241404(R) (2001).
  - [19] R. A. Jishi *et al.*, Chem. Phys. Lett. **209**, 77 (1993). For other calculated phonon dispersion curve, see G. Benedek and G. Onida, Phys. Rev. B **47**, 16471 (1993).